Region-1 and Chapman-Ferraro Current Variations with Solar Wind Conditions

Ava Dupré
University of Michigan

Abstract
Magnetic reconnection between the IMF and the Earth's intrinsic dayside magnetic field is a primary source of energy that causes geomagnetic storms. In particular, the IMF direction (Bz) plays the most important role in whether reconnection occurs. A northward magnetic field does not reconnect with Earth's field since both field lines flow in the same direction. However, a southward magnetic field initiates reconnection and dramatically alters the geometry of the magnetosphere after a short length of time. It has been observed through empirical analysis that reconnection is limited by the increase of Chapman-Ferraro (CF) currents on the dayside magnetic field of Earth. These currents are induced by the accompanying electric field within the solar wind. The greater the magnitude of the solar wind electric field, the greater the generated CF currents. As the magnetosphere transfer energy throughout the system, Region-1 (R1) currents associated with plasma sheet currents dominate the pole regions of the magnetosphere by shifting the field lines sunward and essentially close around the dayside magnetic field of Earth. The induced magnetic field of this current is in the same direction as the southward IMF. Using BATS-R-US, part of the Space Weather Modeling Framework (SWMF), and run results from the Community Coordinated Modeling Center (CCMC), this study will compare a variety of solar wind conditions for a closer look at this process.

Introduction
This study begins with a few questions about the region of Earth's magnetic field on the dayside. We want to see how solar wind conditions affect the magnetopause standoff distance, how R1 and CF currents evolve with a variety of solar wind conditions and how those currents affect the geometry of Earth's magnetic field.

Many models have been studied to predict the magnetopause standoff distance. Parameters such as dynamic solar wind pressure and IMF are typically incorporated into these models. [*Shue et al*., 1997] formulated a model independent of the IMF. These models do not account for the high-latitude variations in distance but focus on the nose region of the magnetosphere. The approach here is such that an assumption is made about the solar wind dependent magnetopause location; that the CF and R1 current systems will be visible in 2D contour plots generated by previous model runs at the CCMC.

[*Siscoe et al*., 2004] performed a study on four different ideas to account for transpolar potential saturation. Dipole field reduction at the subsolar magnetopause [*Hill et al*., 1976], dimple formation at the stagnation point [*Ridley*, 2001; *Raeder* et al., 2001], widening of the magnetosheath relieving the tendency to force reconnection at the magnetopause and ram pressure saturation. All four of these approaches include a role of the R1 current system. The study discussed here is particularly interested in the dimple formation at the stagnation point of the dayside magnetopause. The thought behind the second of the listed mechanisms is that as the R1 system strengthens, it generates a perturbation magnetic field that produces a dimple in the

magnetopause at or near the low-latitude site of magnetic reconnection. The R1 system weakens the magnetic field at the dayside magnetopause at low latitudes, but at the same time it intensifies the field at high latitudes at the dayside magnetopause. Thus the magnetopause develops high-latitude shoulders and a low latitude dimple. Dimples tend to fill with stagnated plasma, which puts a buffer between the boundary and the flow [e.g., *Spreiter and Summers*, 1967]. As a dimple begins to form, it is theorized that the solar wind might begin to lose its reconnection grip on the magnetopause, thus halting further increase of convection.

Another view of dimple formation comes from the vacuum field superposition. If a uniform southward magnetic field is superposed on the Earth's dipole field, the geometry of field lines around the equatorial line where reconnection occurs can be described as dimple-like. Dimple geometry is natural when the IMF is directed southward. However, dimple geometry does not typically happen in the real case because the CF field compresses the dipole field and, in effect, presses out the dimple. Under saturation conditions however, CF compression goes away (figure 1). The run results referred to here do not show dimple formation. Magnetohydrodynamic (MHD) simulations have shown to support the dimple mechanism. An extreme case result [*Ridley*, 2003] produced from a BATS-R-US simulation shows the high-latitude shoulders and low-latitude dimple.

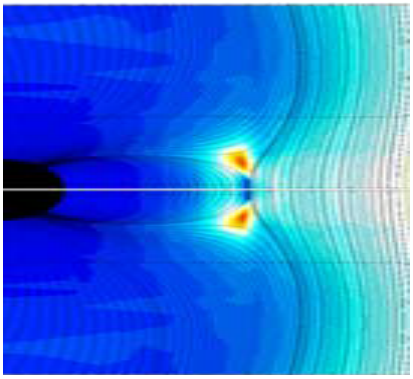

Figure 1: (Ridley, 2003) IMF Bz = -100 nT

The sunward movement of the magnetopause, approximately 7 R_e north and south of the polar-regions, are evident in the above images when compared to quiet time images of the magnetosphere. During a nominal solar wind the magnetopause location is on average 10 R_e (R_e = 1 Earth Radii) outward on the dayside of Earth. Northward IMF accompanied by high dynamic solar wind pressures can compress the magnetosphere resulting in a decreased magnetopause standoff distance. Under those conditions the magnetosphere takes on a streamlined geometry where the high-latitude field lines move towards the night-side and closer to the equatorial line. Only as a reference to R1 and CF current development will northward IMF and high dynamic solar wind pressures be discussed here.

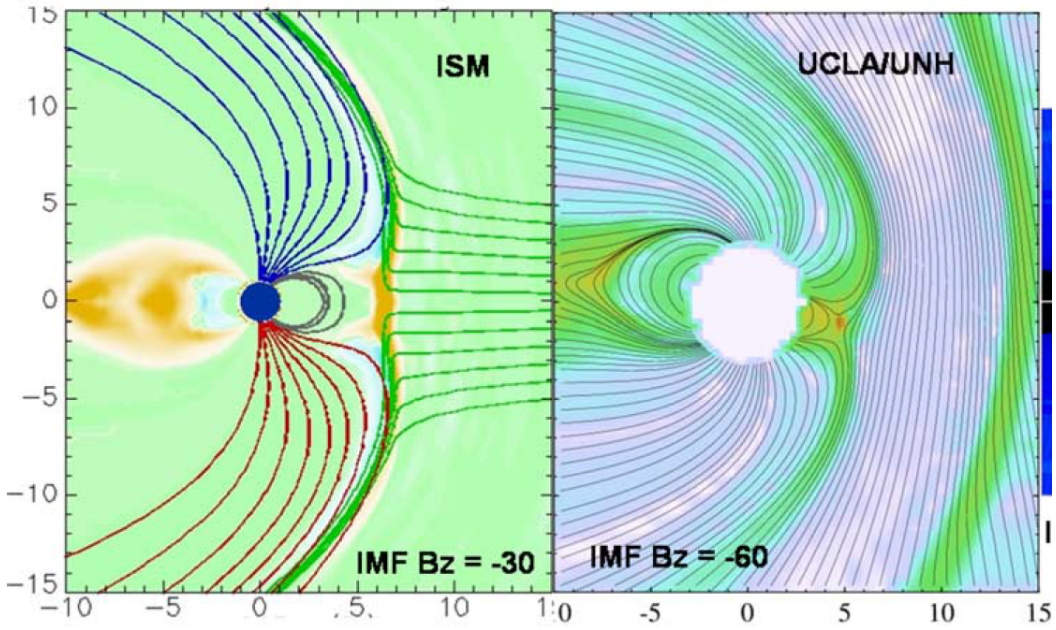

Figure 2: MHD simulations

Methodology

Utilizing the vast resources at CCMC in conjunction with the Virtual Modeling Repository (VMR) allowed for a reasonable investigation into the dynamics of magnetopause and magnetosphere variations as a function of solar wind in-situ data. The SWMF contains 9 modules to cover various regions between the sun and the earth. Here, we look at the global magnetosphere (GM) and ionosphere electrodynamics (IE) modules which include BATS-R-US plus the Rice Convection Model (RCM). The RCM modifies the plasma pressure distribution in the inner magnetosphere and changes the resulting field-aligned currents in the ionosphere yielding more realistic R1 currents. The web interface for visualizing run results was the primary tool for this study. In particular, data time choices, plot region options, quantity choices i.e., currents, velocity, pressure etc., plot mode (3D, 2D contour for example) and ASCI text files allowed for a detailed look at the near-Earth space environment generated by the models.

Three different sets of solar wind data were considered as initial conditions for the chosen model runs; October 29-30, 2003, January 20-21, 2005 and December 14-15, 2006. Each set contained a unique velocity, proton density and magnetic field variation over time. As mentioned the main focus of this study was to look at how CF currents changed over time along with R1 current variation for the chosen data sets. Using CCMC run results, a visual inspection of the spatial distribution of current within the magnetosphere and at the magnetopause was made possible. The XZ plane was chosen for visual inspection and allowed for a detailed look at R1 and CF currents. The current systems were viewed for all three time periods of interest. Considering solar wind velocity and IMF parameters as the primary indicators of possible geomagnetic storms four plots for each data set were used for this study. Also, Birkland current plots from the RCM module and accompanying text files produced allowed for a systematic look at the current system's evolution. The text files allowed for a qualitative analysis of the magnetopause standoff distance as a function of CF current strength given by visual analysis of the 2D contour plots shown below. Similarly, the high-latitude regions of the magnetopause are considered as a function of R1 currents.

Results

For the October data set, containing a southward IMF of ~-60 nT and 2000+ km/s solar wind velocity, the theoretical sunward motion of enhanced R1 currents which are believed to limit dayside reconnection leading to geomagnetic storms are evident. As a supplement to contour plots, polar region Birkland current plots are also shown to further understand R1 currents and ring current evolution as solar wind conditions vary over time. From the center of each plot representing the northern hemisphere each ring is 10^0 latitude. Current plots at the R1 and CF regions extrapolated from visual inspection of the contour plots reveal an increase/decrease with solar wind driving over time. In some instances, the magnetopause currents virtually disappear, especially so during the main phase of the October storm.

During the October period considered, the solar wind was highly variable as the Sun was very active for a number of days around Halloween of the year 2003. Initially, figure 4 shows a magnetopause distance of ~8-9 R_e and the Birkland current polar plot shows a relatively high current. In this study, a high-latitude current of +/- 3 $\mu A/m^2$ is relatively strong while a current of +/- 1 $\mu A/m^2$ is relatively weak. Birkland currents shown here are a combination of R1 and R2 currents where R2 currents are connected to the ring current formation during geomagnetic storms. R2 currents flow from dusk to dawn while R1 currents flow from dawn to dusk across the polar regions.

In figure 3, which represents the beginning of the data set for the October, 2003 time period, the current density is strongest at the magnetopause along or near the equatorial line depending on the axis tilt of the selected times. Here, the magnetopause is located at approximately 8-9 R_e. Note the small dip between 10-12 R_e which represents magnetosheath currents. Also, at this time, the polar region plot shows a R2 dominated current system taking the red/yellow color to be flowing into the page and the blue to represent current flowing out of the page. Around 08:00 UT, the IMF turns southward to ~ 60 nT and the velocity jumps to ~2500 km/s as shown in the solar wind data obtained from CCMC. Figure 5 shows the magnetosphere geometry changes after 10 hours of the main phase of a geomagnetic storm which have been observed to last 2-3 hours on average. However, as stated, this time period of interest contained great variation while the Sun was active which may have led to a longer recovery time.

Notice how the high-latitude shoulders have moved sunward and CF current strength has decreased (figure 5, left panel). The same color scale holds for all plots in this study made possible by the color range options on the CCMC web interface. The polar plots reveal a dramatic increase in currents approximately 3 times greater than initial conditions. Considering just this moment of model produced data it seems the current flow across the north pole goes from local noon to local midnight.

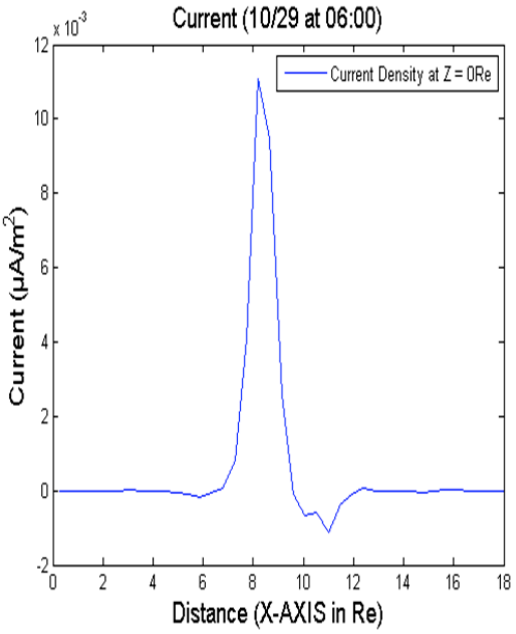

Figure 3: Initial conditions for October

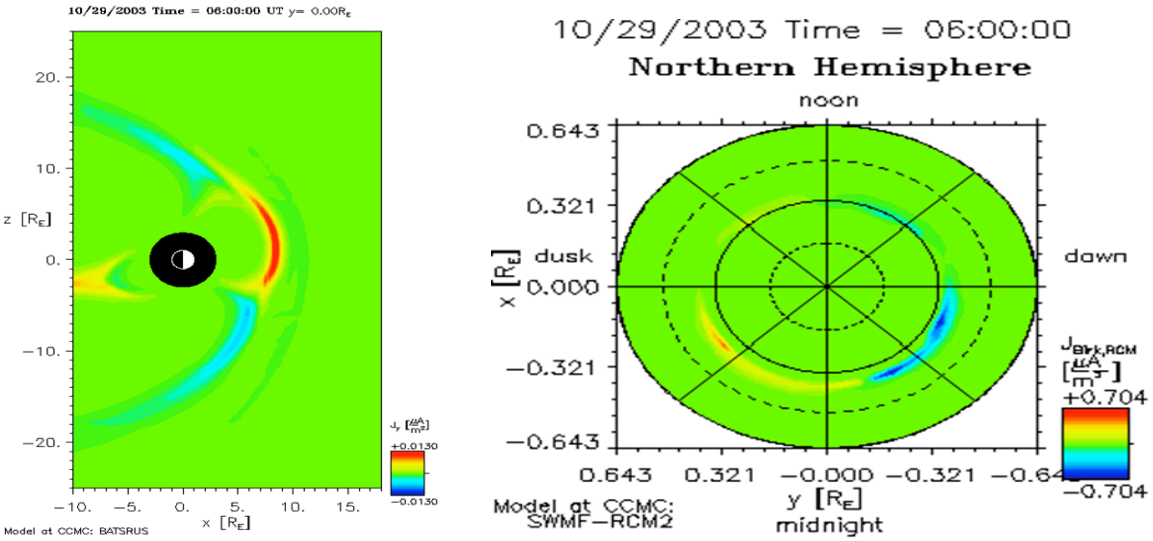

Figure 4: Initial conditions for October data set

To further look into the conditions at the magnetopause a sensitivity study was conducted. Of interest was how current density changed moving from the north most projection of the magnetopause distance to south. For example, referring to figure 4 (left panel), the z-axis extends from 25 to -25 R_e. A line extending from the both boundaries along the x-axis magnetopause boundary is considered as a way to look at velocity, magnetic fields and particle density in this region. In general, the results show high density, low velocity and changes in magnetic field strength and/or direction stepping through the z-axis range. For the October run, figures 6 and 7 show these results. For most instances, the below images are consistent for all three data sets. The current density is shown to be greatest at the magnetopause along the equatorial line and can

be related here as a stagnation point. This stagnation point is said to be where the dimple forms. The rotation in magnetic field with increase in current reveals a weakened field with respect to the ambient solar wind. The ambient solar wind for example would exist outside of the +/- 20 R_e z-axis range.

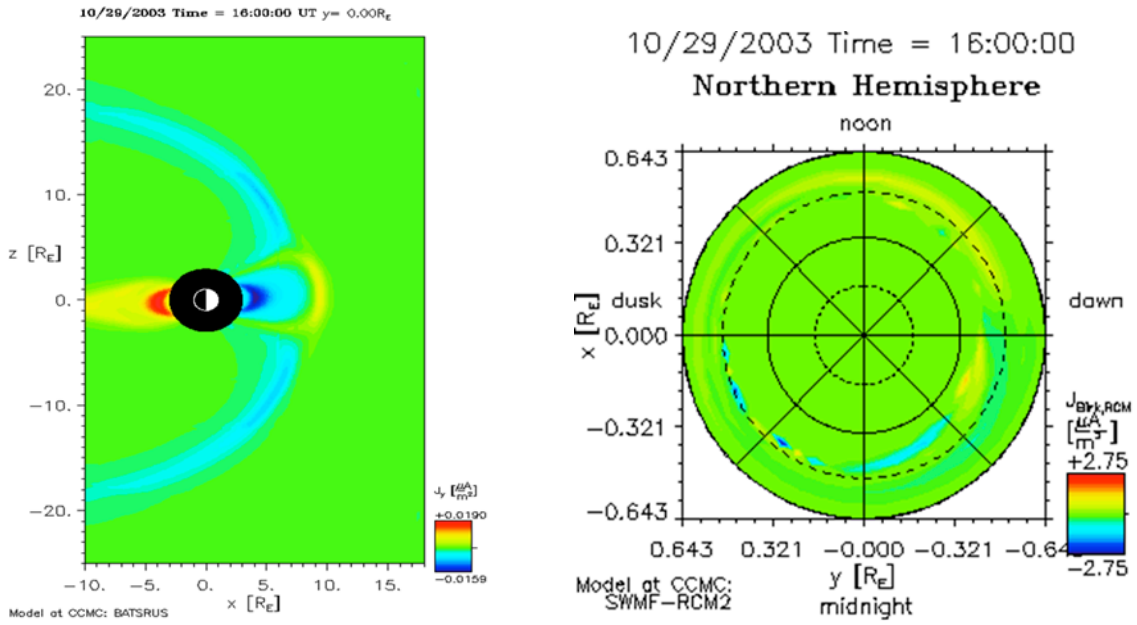

Figure 5: October, 10 hours after onset of southward Bz

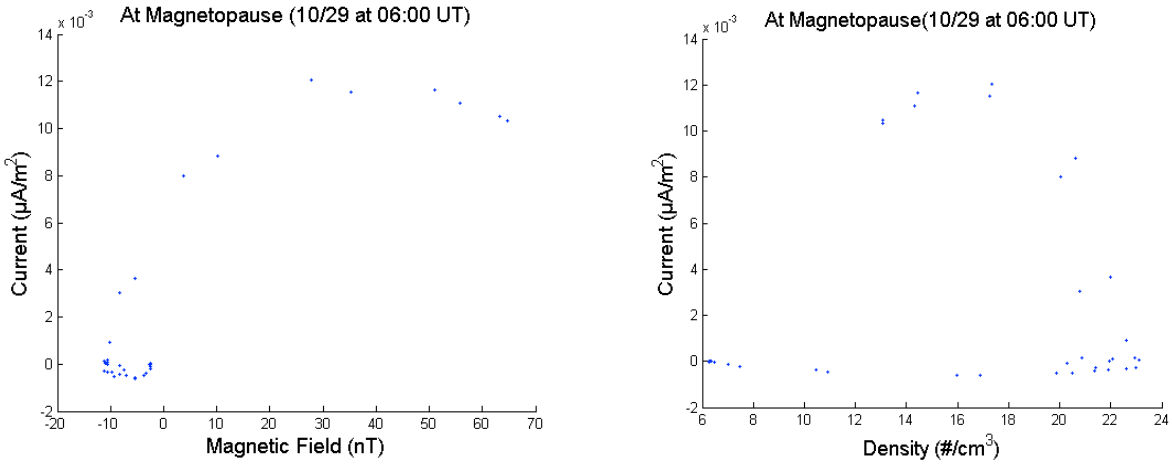

Figure 6: Stagnation point, October initial conditions

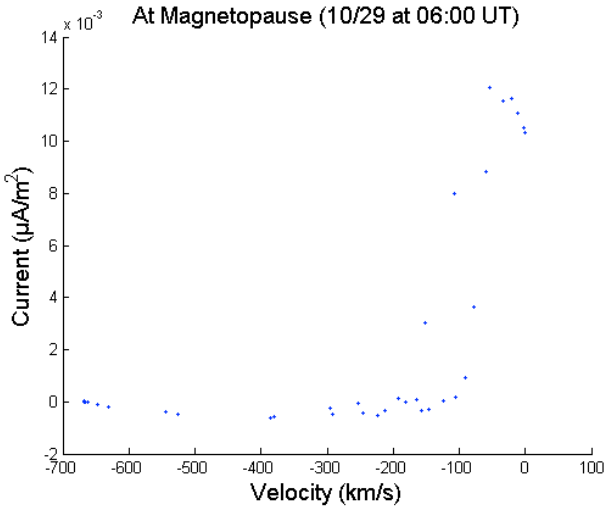

Figure 7: Stagnation point

During the January period considered, the solar wind velocity reveals a shock region with a jump up to ~900 km/s. The proton density shows an increase and slowly trails off and the IMF goes southward with a variable period shortly after. Initially, figure 6 shows a magnetopause distance of ~10 R_e. For this particular run, no Birkland current polar plot was available. Around 17:30 UT, the IMF turns southward to ~ 10 nT.

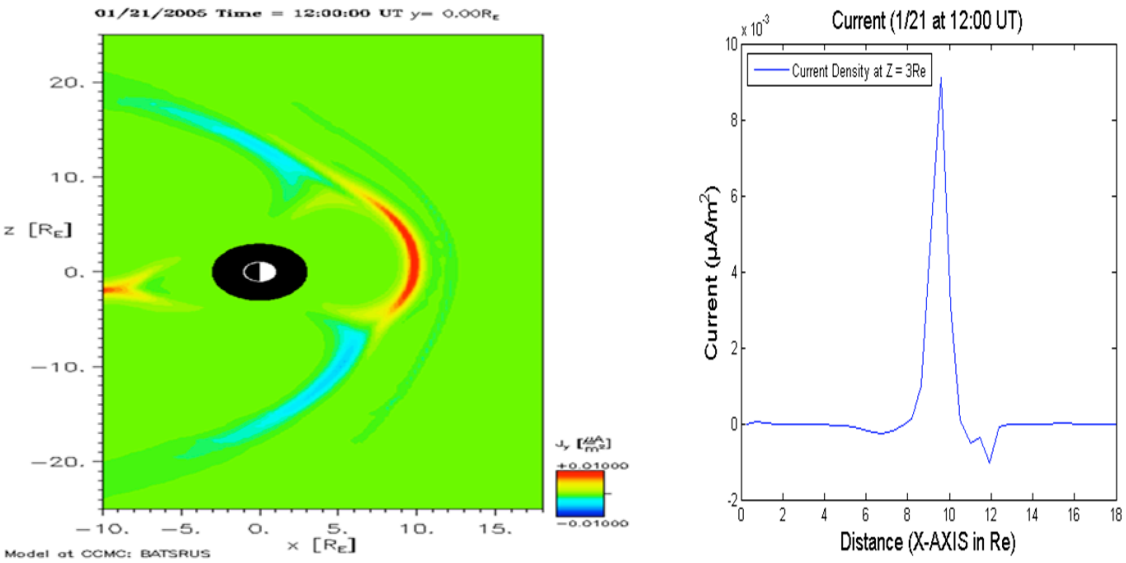

Figure 8: Initial conditions for January

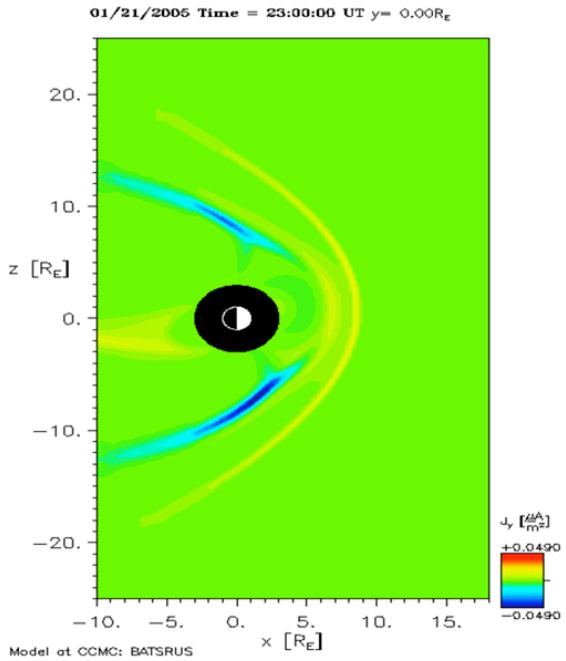

Figure 9: 5 hours after southward IMF (January)

In the January data set, the IMF rotates northward fairly quickly. Figure 9 shows ~5 hours after a southward IMF hits the magnetosphere. Again, we see a dramatic decrease in the CF current region and increase in the R1 current region. Note the high dynamic solar wind pressure/northward IMF shape of the magnetosphere at this time. Figures 10 and 11 show a stagnation point following the method described for the October data set.

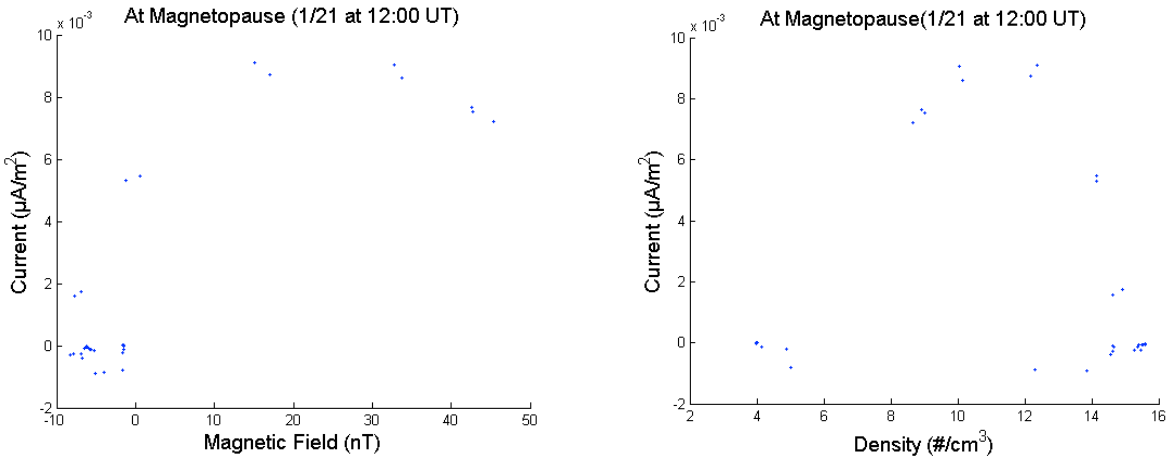

Figure 10: January stagnation

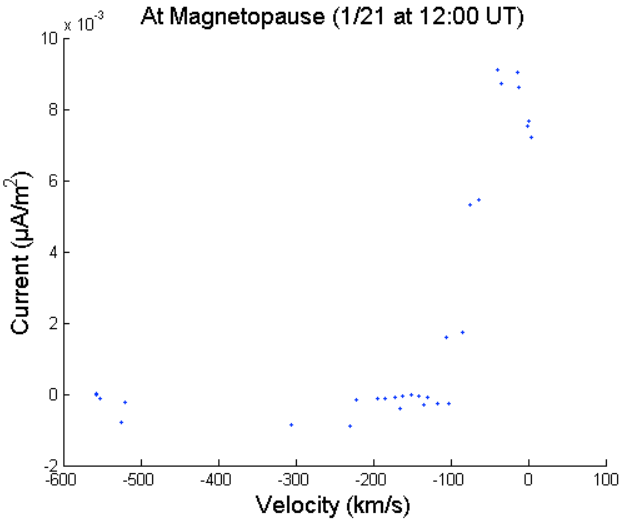

Figure 11: January stagnation

For the December run, the initial solar wind velocity is similar to the January data set beginning around 600 km/s. This time the proton density and IMF are highly variable as seen in the solar wind satellite data. The magnetopause is observed to be ~10 R_e as shown in figure 10.

12 hours after initial conditions the IMF turns southward ~20 nT. To look at the development of R1 and CF currents we took a look at a period of time where their respective maximums and minimums had yet to be reached. As can be seen, the high-latitude shoulders have begun to develop yet the CF current is still relatively strong (figure 13, left panel). For variation, the sensitivity plots are from the development stage in figure 13. In figures 14 and 15, the same low velocity and change in magnetic field direction can be seen but this time the region is slightly less dense.

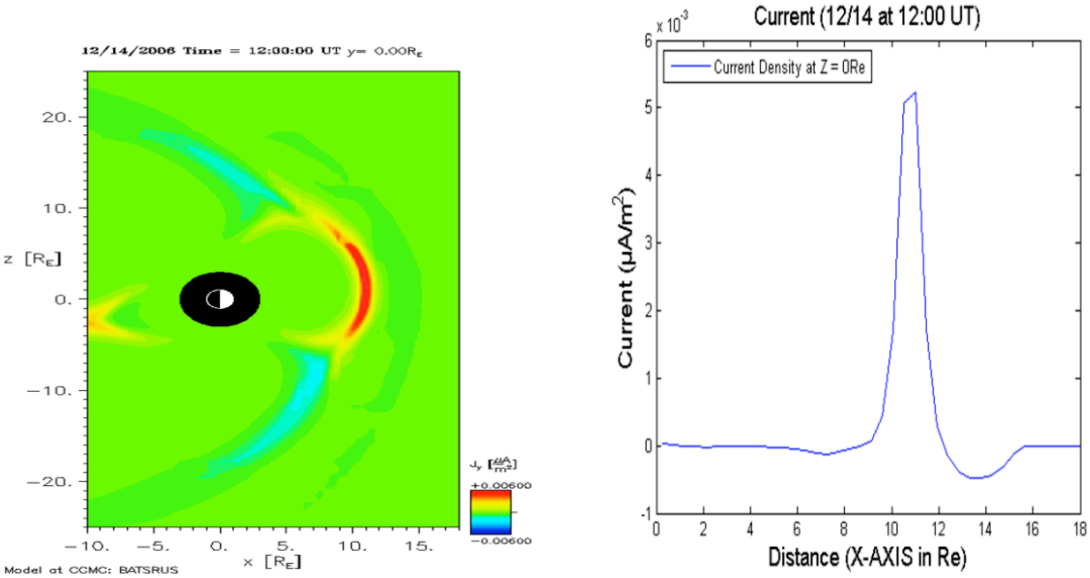

Figure 12: December initial conditions

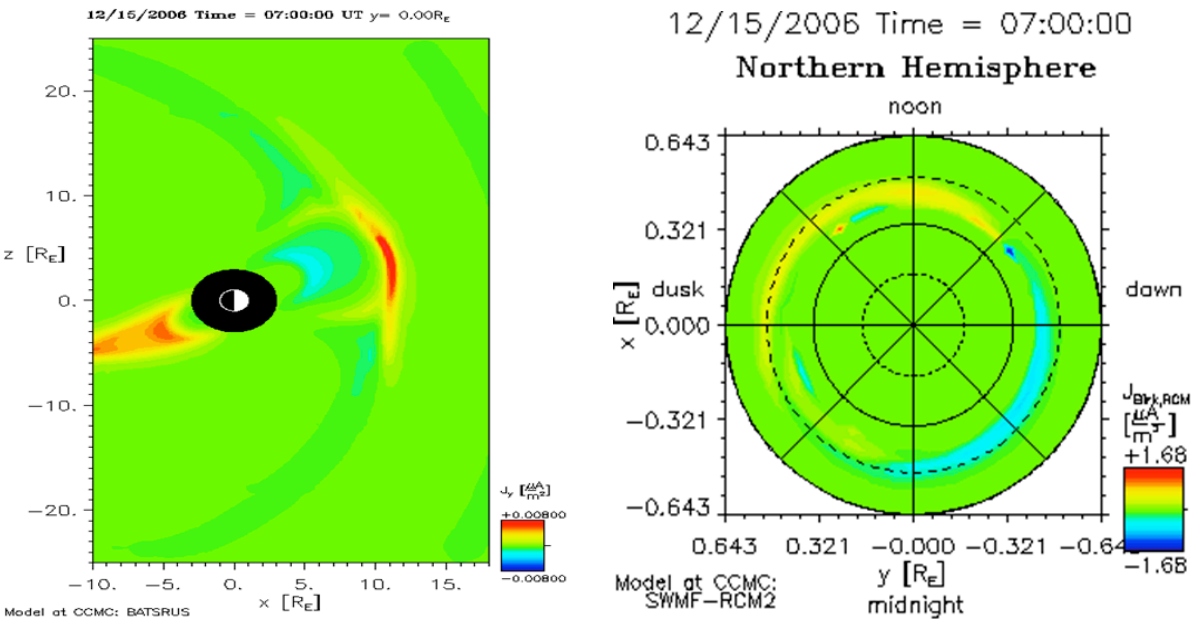

Figure 13: December, 12 hours after initial conditions

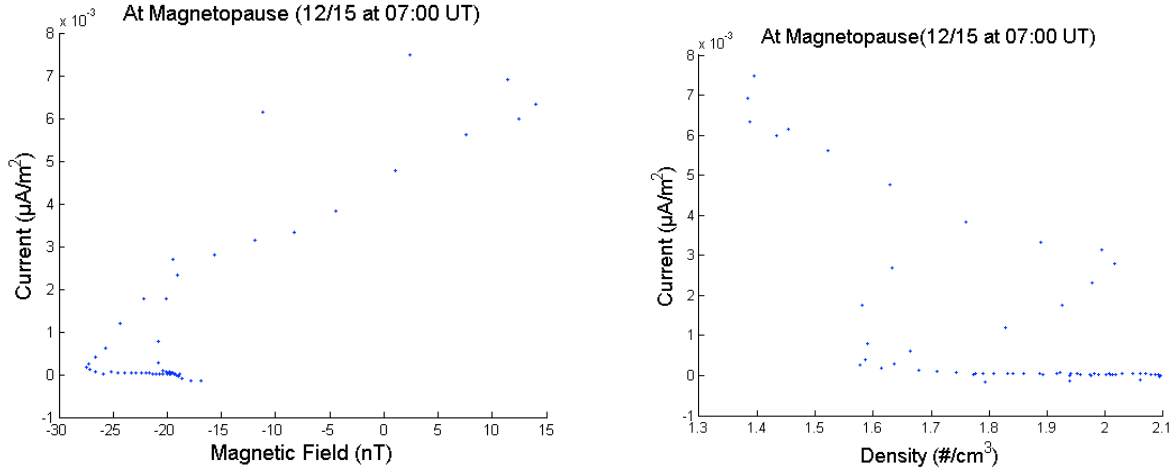

Figure 14: December stagnation

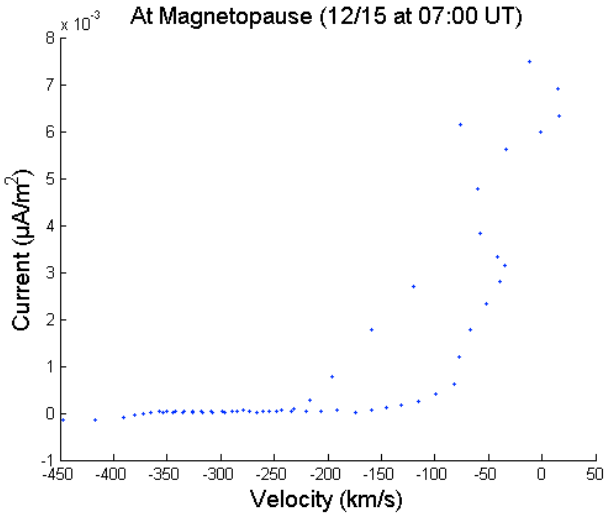

Figure 15: December stagnation

It should be noted that the solar wind data considered for this data set may not consist of entirely upstream values. Comparing the data sets given for the runs considered with ACE data for the same time periods showed inconsistencies in all of the parameters chosen for the sensitivity portion of this study.

Conclusions

It can be seen that for a variety of solar wind conditions that contain a southward IMF the geometry of the magnetosphere changes with evolving current systems associated with geomagnetic storms. The second mechanism presented in the introduction, dimple formation at the equatorial line, a stagnation point and the associated high-latitude sunward movement of the magnetopause is supported from this study.

The January data contained a rotation of the IMF from south to north. The shoulder regions of the magnetosphere did not move forward in this case suggesting dynamic solar wind pressure dominated the later stages of the initial solar storm conditions. Additionally, [*Guo, X.C. et al.,* 2008] presented results from MHD simulations that show currents generated in the bow shock/magnetosheath region are the main driver to R1 current strengthening under strong southward IMF conditions. As can be seen in the January set (figure 9), there are currents flowing in the sheath region and the R1 current regions are very strong at ~0.04 $\mu A/m^2$. This current strength is twice that of the October run during the peak sunward motion of the magnetosphere shoulder region (at least for the referenced plots for this study where current values range from +/- 0.006 to +/- 0.04 $\mu A/m^2$ on the magnetosphere plots). Based on the results of this study which considers very small windows of time and highly variable solar wind conditions it would be best to perform a more comprehensive analysis before a substantial conclusion can be made about the effects of induced magnetic fields associated with the current systems referred to throughout this paper.

Appendix

Community Coordinated Modeling Center
http://ccmc.gsfc.nasa.gov/

Cravens, Thomas E. *Physics of solar system plasmas,* Cambridge University Press (2004)

Guo, X.C., C. Wang, Y. Q. Hu and J. R. Kan Geophysical Institute, University of Alaska Fairbanks, Fairbanks, Alaska, USA *Bow shock contributions to region 1 field-aligned current: A new result from global MHD simulations* GEOPHYSICAL RESEARCH LETTERS, VOL. 35, 2008 doi:10.1029/2007GL032713

Hill, T. W., A. J. Dessler, and R. A. Wolf (1976), *Mercury and Mars: The role of ionospheric conductivity in the acceleration of magnetospheric particles,* Geophys. Res. Lett., 3, 429– 432.

J-H. Shue, J.K. Chao, H.C. Fu, C.T. Russell, P. Song, K.K. Khurana, H.J. Singer *A new functional form to study the solar wind control of the magnetopause size and shape* J. Geophys. Res., 102 (1997), pp. 9497–9511

Raeder, J., Y. L. Wang, T. J. Fuller-Rowell, and H. J. Singer (2001), *Global simulation of space weather effects of the Bastille Day storm*, Sol. Phys., 204, 325.

Ridley, A. (2001), BATS-R-US simulation of CPVP, paper presented at GEM Mini-workshop, Natl. Sci. Found., San Francisco, Calif.

Ridley, A. (2003), *The saturation of the ionospheric cross polar cap potential and the magnetospheric configuration during extreme solar wind and IMF conditions*, paper presented at Yosemite Conference-Workshop: The Dayside Magnetosphere and Cusp, NASA, Yosemite Natl. Park, Calif.

Siscoe, G., Raeder, J. and Ridley, A.J *Transpolar potential saturation models compared* Journal of geophysical research vol 109 doi: 10.1029/2003JAO10318, 2004

Spreiter, J. R., and A. L. Summers (1967), *On conditions near the neutral points on the magnetosphere boundary,* Planet. Space Sci., 15, 787– 798.

Virtual Modeling Repository
http://vmr.engin.umich.edu/